Relaxation times of colloidal iron platinum in polymer matrixes†‡

Maria Puerto Morales,*[a] Matthieu F. Bédard,[bc] Alejandro G. Roca,[a] Patricia de la Presa,[d] Antonio Hernando,[d] Feng Zhang,[e] Marco Zanella,[e] Abbasi Azhar Zahoor,[e] Gleb B. Sukhorukov,[c] Loretta L. del Mercato[e] and Wolfgang J. Parak*[ef]

Received 1st April 2009, Accepted 29th May 2009
First published as an Advance Article on the web 13th July 2009
DOI: 10.1039/b906455a

Colloidal magnetic iron platinum nanoparticles were embedded at different densities into the walls of polyelectrolyte multilayer capsules. Changes in their magnetic properties such as relaxivities as a function of average distances between the magnetic nanoparticles were investigated and their properties for magnetic resonance imaging discussed.

Introduction

Magnetic particles are interesting as contrast agents for magnetic resonance imaging (MRI). MRI is a non-invasive technique based on the variation of the water proton relaxation time from one tissue to another. Different chemical compounds have been used as contrast agents to enhance the contrast between normal and diseased tissues, to indicate organ function or blood flow.[1] Gadolinium (Gd)-based organometallic complexes provide high contrast for T_1-imaging, while iron (Fe)-containing nanoparticles have been proven to provide good contrast for T_2-imaging.[2,3] Magnetic particles provide good imaging contrast capabilities for MRI because the T_1 and T_2 relaxation times are very sensitive to changes in local field gradients created by the superparamagnetic particles that accelerate the loss of phase coherence of the spins of nearby protons contributing to the MR signal (*e.g.* from surrounding water molecules). Changes in the relaxation times T_1 and T_2 depends on both material composition and on the size of the particles.[4]

Size dependence of the nanoparticles has been extensively demonstrated, both experimentally and theoretically, since magnetic colloidal nanoparticles can be synthesized with excellent size distribution and shape control.[5–12] However, since the magnetic moments of magnetic nanoparticles are strongly affected by environmental factors, introducing such nanoparticles in a different environment may have serious implications on their MRI potential. In this sense, if individual colloidal nanoparticles aggregate to ill-defined complexes their contrast providing properties change significantly.[13] Magnetic nanoparticles can be embedded into matrixes in order to improve their contrast providing properties.[14] Whereas size dependence of contrasting has been investigated in much detail, there is only a limited number of studies available in which the inter-particle distance on contrasting is studied.[14] This is mainly due to the fact that it is technologically complicated to vary the mean inter-particle distance without changing other parameters such as the composition of the matrix in which the particles are embedded or the surface chemistry of the particles. In this study, we introduce polyelectrolyte capsules as a convenient matrix system which allows for the integration of colloidal nanoparticles at controlled nanoparticle density and thus provides a good system for studying the inter-particle distance dependent contrasting.

Polyelectrolyte capsules are constructed using the layer-by-layer assembly (LbL) approach according to which oppositely charged polymers are alternatively added to a charged surface.[15] Growth of a multilayered film is possible because each addition of a polyelectrolyte layer results in some uncompensated charges that permit an oppositely charged polymer to deposit.[16] Once the desired LbL composition is obtained, the colloidal template was decomposed resulting in hollow polymeric capsules.[17,18] As the different layers of polyelectrolyte microcapsules are held together primarily by electrostatic forces, charged nanoparticles (or other charged macromolecules) can be integrated into the polyelectrolyte network.[19–24] In this way capsules with magnetic Fe-based nanoparticles within their polyelectrolyte walls have been synthesized.[25–28] Such capsules were used for targeted drug delivery, in which capsules could be directed to target locations with magnetic field gradients.[27,29] Besides targeted delivery and visualization, magnetic nanoparticles were also used as an agent to remotely open microcapsules using an alternating magnetic field and inducing nanoparticles embedded in the capsule shell to rotate, damaging the latter and allowing the capsule to release encapsulated substances.[28] Microcapsule technology is also attractive due to the many physical parameters that can be finely-tuned, such as shell thickness and roughness. Capsules are due to their controlled step-by-step construction also an ideal matrix for

[a]*Instituto de Ciencia de Materiales de Madrid, CSIC, C) Sor Juana Inés de la Cruz 3, Campus de Cantoblanco, 28049 Madrid, Spain. E-mail: Puerto@icmm.csic.es*
[b]*Max-Planck Institute of Colloids and Interfaces, Potsdam 14424, Germany*
[c]*School of Engineering and Materials Science, Queen Mary, University of London, London, UK E1 4NS*
[d]*Instituto de Magnetismo Aplicado, UCM-ADIF-CSIC, 28230 Las Rozas (Madrid), Spain*
[e]*Fachbereich Physik, Philipps Universität Marburg, Marburg, Germany. E-mail: wolfgang.parak@physik.uni-marburg.de*
[f]*Wissenschaftliches Zentrum für Materialwissenschaften, Philipps Universität Marburg, Marburg, Germany*

† This paper is part of a *Journal of Materials Chemistry* theme issue on inorganic nanoparticles for biological sensing, imaging, and therapeutics. Guest editor: Jinwoo Cheon.

‡ Electronic supplementary information (ESI) available: Additional data for the characterization of the FePt particles, and the determination of the number of FePt particles per capsule. See DOI: 10.1039/b906455a

changing the mean distance between magnetic particles. Charge–charge repulsion between nanoparticles which are deposited at the surface of a polyelectrolyte film helps maintain a homogeneous distribution in the final capsule construction.[22] In the work presented here capsules were loaded with three different concentrations of magnetic nanoparticles and their effect on T_1 and T_2 relaxation was compared to that of free nanoparticles.

Materials and methods

FePt nanoparticle synthesis

Synthesis of hydrophobic FePt nanoparticles. We followed the recipe previously reported by Sun *et al.*[5] Briefly, in a 50 ml three-neck flask, 10 ml of octyl ether, 95mg of platinum acetylacetonate and 195 mg of hexadecanediol were mixed under nitrogen atmosphere. Temperature was raised up to 100 °C until the solution turned into a clear translucent yellow color. Oleic acid (0.08 ml), oleyl amine (0.08 ml) and iron pentacarbonyl (0.06 ml) were quickly injected under vigorous stirring and the temperature was raised to 280 °C with a rate of 12 °C/min, then the solution was left at that temperature for 15 minutes before removing the heating mantle. Nanoparticles were then washed with a mixture of methanol and ethyl acetate and redispersed in fresh chloroform. The synthesis yielded nearly monodisperse nanoparticles which were characterized by transmission electron microscopy (TEM). In a next step the hydrophobic nanoparticles were transferred to aqueous solution by coating them with an amphiphilic polymer.

Synthesis of the amphiphilic polymer. The synthesis of the amphiphilic polymer has been reported previously.[30,31] Briefly, 2.70 g (15 mmol) of dodecylamine (DoCA, 98%, Sigma, # D22,220-8) was firstly dissolved in 100 ml tetrahydrofurane anhydrous (THF, ≥99.9%, Aldrich, #186562) in a round flask. After dodecylamine dissolved well, the solution was poured into another round flask with 3.084 g (20 mmol motifs, one polymer molecule has about 39 motifs) powder of poly(isobutylene-alt-maleic anhydride, average Mw ~6,000 g/mol, Sigma, #531278). This mixture was sonicated for several seconds (~20 s), and then heated to 55–60 °C for 1 hour under stirring conditions. Afterwards, the solution was concentrated to 30–40 ml by evaporation of THF solvent and left stirring overnight. Finally, the solution was completely dried by evaporation and redissolved in 40ml anhydrous chloroform to a final concentration of 0.5 M of polymer motifs.

Coating of the hydrophobic FePt particles with the amphiphilic polymer. The polymer coating procedure has been described previously.[30,31] Briefly, solutions of polymers were mixed with FePt nanoparticle solution in a round flask. The polymer was kept in excess by using 200 motifs per nm^2 of particle's surface to obtain the best size distribution. By slowly evaporating the solvents completely, the particles with polymer were redissolved in SBB (50 mM sodium borate, pH 12) buffer.

Purification of the water-soluble polymer coated FePt particles. Polymer coated FePt nanoparticles were purified by size exclusion chromatography using a Sephacryl S300 HR gel column (GE Healthcare, #17-0599-10) connected with a HPLC system (Agilent 1100). Before and after the purification, the polymer coated FePt nanoparticle samples were concentrated by ultrafilters (100kD MWCO, Millipore) followed by additional filtering with 0.2 μm filters (Millipore) to get rid of any possible big aggregates. The purified samples were stocked in SBBS buffer (50mM sodium borate, 100mM NaCl, pH 9.0) finally.

Capsule synthesis

Preparation of Silica Templates. The fabrication of $(PDADMAC/PSS)_4$ microcapsules was done on 4.78 μm silica particles (Microparticles GmbH, Germany) using the Layer-by-Layer deposition technique.[23] Typically, 1 mL of template SiO_2 particles solution were first cleaned from stabilizers in a sonication bath after resuspending them in a 1:1 solution of water and isopropanol.

LbL assembly of polyelectrolyte capsules. Solutions of poly(diallyldimethylammonium chloride) (PDADMAC, Sigma-Aldrich, 200–350 kDa) (2 mg/mL, 0.5 M NaCl) and poly(styrenesulfonate, sodium salt) (PSS, Sigma-Aldrich, 70 kDa) (2 mg/mL, 0.5 M NaCl) were prepared without further purification. Silica templates with an average diameter of 4.78 μm were treated alternatively with 3 layers of polyelectrolytes beginning with PDADMAC and ending with PDADMAC. At layers 3 and 5 (PDADMAC), SiO_2 templates were re-suspended in a mixture of water and polymer-coated FePt nanoparticles suspension with desired concentration, while gently stirring. A total of four PDADMAC/PSS bilayers of polyelectrolytes were used to coat the silica templates. Particles needed to be treated in a sonication bath after each step of assembly in order to reduce the tendency of the samples to aggregate. When the desired multilayer structure was obtained, the templates were dissolved in HF (0.3 M) solution, and the sample was then washed with water until the pH of the solution reaches above 5. In total, 3 types of polymeric microcapsules were prepared using three different concentrations of FePt nanoparticles (low, medium and high), moreover one sample made of capsules without FePt nanoparticles was fabricated as control. A schematic of the samples analyzed in this work are displayed in Fig. 1.

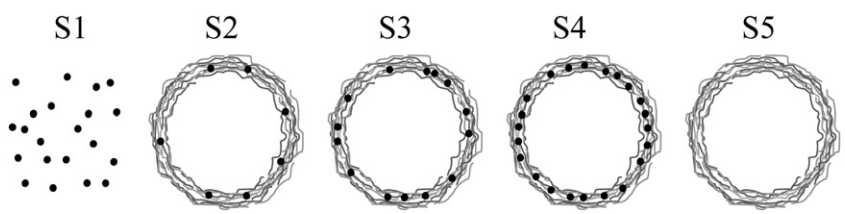

Fig. 1 Five different samples were prepared. Free FePt particles (S1), polyelectrolyte capsules with a low (S2), medium (S3), and high (S4) concentration of FePt particles, and polyelectrolyte capsules without FePt particles (S5).

Capsule characterization

Determination of Microcapsule Diameter. To visualize the microshells by laser scanning confocal microscopy (LSCM) the capsules were made fluorescent by the addition of a drop of 10^{-7} M solution of rhodamine 6G. A Leica TCS SP confocal scanning system (Leica, Germany) equipped with a 100x/1.4-0.7 oil immersion objective was used for measurements. The average capsule diameter for each sample was determined by measuring the wall-to-wall diameter at the largest point for at least 30 capsules per sample. The diameters were determined to be 4.9 μm ± 0.2, 4.8 μm ± 0.2, 5.0 μm ± 0.3 and 4.8μm ± 0.2 for samples S2 to S5, respectively. The diameters were therefore not significantly different.

Number of FePt nanoparticles per capsule. The concentration of capsules was directly determined by taking an aliquot of solution and counting the number of capsules with an optical microscope in phase-contrast mode and was determined to be around 10^9 capsules per mL. The counted numbers were generated by averaging the number of capsules contained in 6 aliquots of a dilution of each sample leading to a standard deviation of around 10%. The concentration of iron atoms in each sample was determined with elemental analysis. For this purpose samples were digested with nitric acid to oxidize the organic coating and then, with hydrochloride acid to dissolve the iron. The Fe concentration was then measured in a plasma emission spectrometer (ICP) PERKIN ELMER OPTIMA 2100 DV. We estimated that each FePt nanoparticle with a diameter of 3.2 ± 0.4 nm as determined by TEM comprises approximately 288 ± 91 Fe atoms.[32] Using this number the FePt nanoparticle concentration of each solution is 1/288-th of the measured iron concentration. By knowing the FePt nanoparticle and the capsule concentration of each solution the number of FePt nanoparticles embedded per capsule was determined, by assuming that all FePt nanoparticles were actually bound to the capsules. In this way we estimated the number of $2.6 \times 10^8 \pm 0.9 \times 10^8$, $3.2 \times 10^8 \pm 1.1 \times 10^8$, and $6.6 \times 10^8 \pm 2.3 \times 10^8$ FePt nanoparticles per polymer capsules for the samples S2, S3, and S4, respectively (cf. Table 1).

Structural characterization of capsules. Transmission electron microscopy (TEM) was done using a Zeiss Omega EM 912 at an operating voltage of 120 kV. Hereby the FePt nanoparticles provide strong contrast against the polymer layers.

Magnetic and relaxometric characterization

For each type of sample (S1–S5) a concentration series of different aliquots was done by dilution. The Fe concentration c(Fe) within each aliquot was determined with elemental analysis using a plasma emission spectrometer (ICP) as described above. Magnetic characterisation of the suspensions (0.1 ml) was carried out by means of a Quantum Design SQUID magnetometer in special closed sample holders. The magnetic characterization consists in hysteresis cycles at 5 Tesla and at 5 K. Relaxometric properties were also investigated for each aliquot by measuring T_1 and T_2 protons relaxation times at different dilutions. The relaxation time measurements were carried out in a MINISPEC MQ60 (Brucker) at 37 °C and a magnetic field of 1.5 T. From the graph of the Fe-concentration dependent relaxation times, the relaxivities r_1 and r_2 were determined for each type of sample.

Results and discussion

Structural analysis

Representative TEM images of capsules containing different concentrations of FePt nanoparticles are shown in Fig. 2 (upper row). The capsules, typically spherical in solution, appear with folds and creases in TEM imaging as a result of drying. The thin and light coloured folds seen in the centre of the capsule in sample S2 indicate that the shell is rather thin. On the other hand, the dark and thicker folds found in S4 indicate relatively thicker capsule walls. It was found by LSCM measurements that all the capsules are approximately the same diameter (∼ 4.9 μm). A magnification of flat areas of capsules from each sample is shown in the lower row. The FePt particles are clearly visible as dark spots. From these images the increasing loading density from sample S2 to S3 and to S4 is also supported by the fact that folds in the dried capsules appear darker and thicker as FePt nanoparticle concentration increases. These observations agree well with the data obtained from elemental analysis. Furthermore the particles show a random distribution in the polymer matrix instead of forming regions of agglomerated particles.

Magnetic and relaxometric properties

Hysteresis curves at 5 T of 0.1 ml suspensions of capsules containing different concentrations of FePt nanoparticles were recorded and a section of the loops for samples S2 and S3 around ±2 Teslas is shown in Fig. 3. The inset in Fig. 3 shows the complete hysteresis loop for sample S3. Sample S4 shows similar magnetic behaviour as sample S3. Room temperature curves are unable to distinguish between capsules because of the low saturation magnetization values at that temperature (0.5 emu/g for pure FePt particles). The magnetic response depends strongly on the FePt concentration in the capsules. For low FePt concentrations (S2), a reversible magnetisation curve is obtained indicating superparamagnetic behaviour at 5 K and lower blocking temperatures. However, for high FePt concentrations (S3 and S4) a hysteresis loop is observed with a coercivity of 800 Oe. These results indicate an increase in the dipolar interactions between particles from sample S2 to sample S3 as expected when encapsulating more FePt particles in a similar size capsule. Saturation magnetisation is reached at lower field for sample S3 as a consequence of the stronger dipolar interactions and is about

Table 1 Number of FePt nanoparticles per capsule for samples S2, S3, S4

sample	S2	S3	S4
FePt NPs/capsule	$2.6 \times 10^8 \pm 0.9 \times 10^8$	$3.2 \times 10^8 \pm 1.1 \times 10^8$	$6.6 \times 10^8 \pm 2.3 \times 10^8$

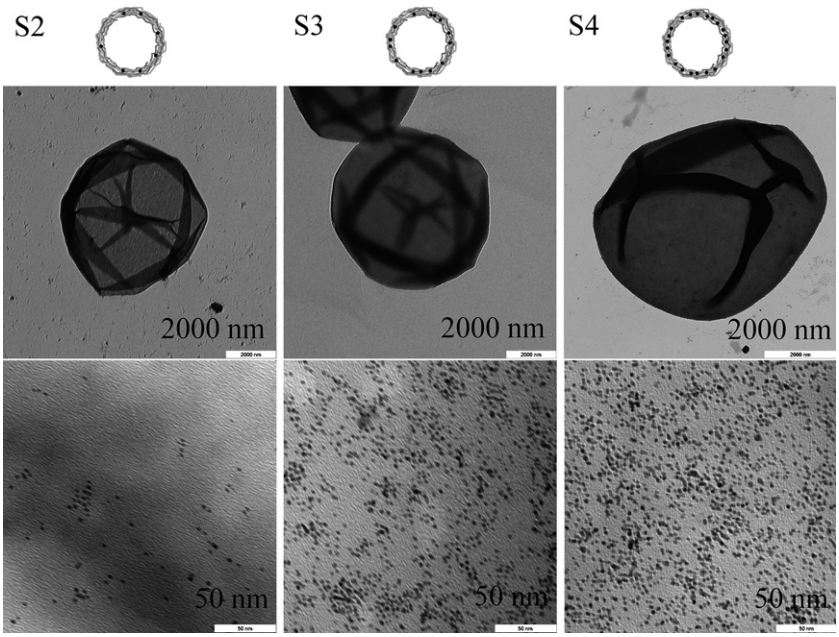

Fig. 2 TEM images in low and high resolution for samples S2, S3, and S4. The low magnification images show individual capsules. The high resolution images are zoomed into the capsule shells and show the distribution of the FePt particles in the capsule wall. The scale bars in the upper and lower row correspond to 2 μm and 50 nm, respectively.

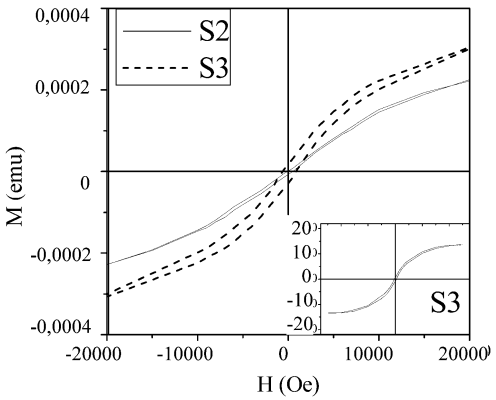

Fig. 3 Hysteresis loops at 5K for S2 and S3 suspensions containing different FePt nanoparticles per capsule.

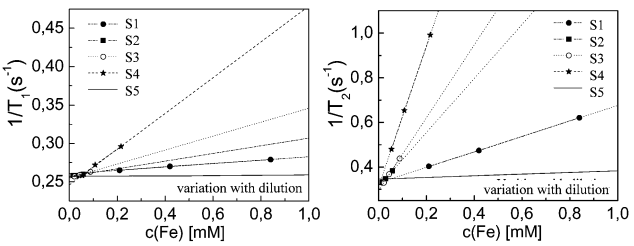

Fig. 4 T_1 and T_2 relaxation times for samples S1–S5 for different dilutions. Concentrations of each diluted aliquot were determined by the amount of iron (c(Fe)) by ICP.

Table 2 r_1 and r_2 relaxivities for samples S1–S4

sample	S1	S2	S3	S4
r_1 [mmol-^{1}s^{-1}]	0.021	0.045	0.092	0.230
r_2 [mmol-^{1}s^{-1}]	0.35	1.18	1.62	3.14
r_2/r_1	16.7	26.2	17.8	13.6

13 emu/g, much smaller than the saturation of FePt bulk but quite similar to the saturation of FePt NPs of same size.[33]

Magnetic interactions between particles are often significant and may even result in superferromagnetic ordering at low temperatures, *i.e.* ordering of the magnetic moments of particles which would be superparamagnetic if they were isolated.[34,35] This explains the magnetic behavior change from superparamagnetism for sample S2 (low concentration, almost isolated particles) to ferromagnetism for sample S3 (S4) (high concentration, interacting particles).

T_1 and T_2 relaxation times were measured for each of the samples for different concentrations by making a dilution series of each sample solidify with agar (5%) (see Fig. 4 and Table 2). For each concentration series the relaxivities $r_{1,2}$ ($s^{-1}mM^{-1}$) were determined according to eqn (1), where, $R_{1,2}$ are the relaxation rates obtained from the relaxation times ($1/T_{1,2}$ [s^{-1}]) and $R^0_{1,2}$ are the relaxation rates in the absence of contrast agent, *i.e.* the agar contribution.

$$R_{1,2} = R^{o}_{1,2} + r_{1,2} \cdot c(Fe) \quad (1)$$

From the data it is evident that embedding FePt particle changes the relaxation time, dependent of the FePt density in the capsule walls. All r_2 values for iron platinum particles are always well below the values for iron oxide magnetic nanoparticles (in agreement with the lower magnetic moment of FePt, 13 emu/g against ~60 emu/g for magnetite nanoparticles). The values for

r_2 are higher when the FePt particles are inside the capsules (S2, S3, S4) compared to the dispersed isolated FePt particles (S1). The r_2 values also increase with the degree of aggregation, *i.e.* $r_2(S2) < r_2(S3) < r_2(S4)$. This clearly demonstrates that relaxation times depend on the particle type (here: FePt), but also on the density in which they are embedded in a matrix.

Differences in relaxivity are due to local field gradients created by the superparamagnetic particles that accelerate the loss of phase coherence of the spins contributing to the MR signal.[1] Both magnetic moments and interactions (controlled by particle size and distribution) are the required parameters to understand the relaxivity data. The moment per FePt particle is expected to be the same in all capsules but interparticle interactions will modify the effective moment in each particle and therefore the field gradient around it affecting the relaxation of nearby water protons.

Relaxivity values for these FePt particles are two orders of magnitude smaller than r_2 values reported for commercial contrast agents based on iron oxide with similar particle size and hydrodynamic sizes of around 150 nm as Endorem. As the aggregate size decreases, r_2 is in these particles reduced from 120 $mmol^{-1}s^{-1}$ for 150 nm of hydrodynamic size to 65 $mmol^{-1}s^{-1}$ for 30 nm and 33 $mmol\text{-}^{1}s^{-1}$ for 7 nm.[36] However, for the FePt particles in capsules, r_2/r_1 values that are indicative of the effectiveness of the contrast, were similar or even higher than the value reported for the commercial iron oxide products ($r_2/r_1 = 2$ for 7nm aggregate size). Very high r_2 values (>200 $mmol^{-1}s^{-1}$) have been reported for other magnetic nanoparticles such as Manganese ferrites and Cobalt ferrites but the contribution from the aggregation state was unclear. It can be concluded that saturation magnetisation, aggregation state and spatial distribution determine the NMR contrast produced by magnetic nanoparticles.

Conclusions

The results of this study point out how important the inter-particle distance for nanoparticle-based for magnetic contrast agents is. Bringing particles together by embedding them into a carrier matrix drastically increases the r_1 and r_2 relaxivities in magnetic resonance imaging. This fact should be taken into account for many studies in literature in which magnetic nanoparticles are suggested as contrast agents for in vivo magnetic resonance imaging. As a matter of fact the majority of magnetic nanoparticles used nowadays have limited colloidal stability. For this reason such particles tend to agglomerate in body fluids, such as blood, due to the present salt content. As shown in this study agglomeration or likewise controlled decrease of the average inter-particle distance can lead to significant changes in relaxation times. In other words, the magnetic properties of particles inside a body might differ greatly in comparison to the values measured under the laboratory conditions described in the present work. Therefore, in our opinion, without keeping exact track about the degree of agglomeration (for example with measurements of the hydrodynamic diameter of the particles[37]) data about relaxivities have to be interpreted with outmost care. As long as the degree of agglomeration is not exactly known and controlled, relaxivities are not stable but are likely to vary according to subsequent further increase of agglomeration upon incubation in body fluids.

Acknowledgements

The authors are grateful to Dr Andrei Skirtach, Dr Almudena Muñoz Javier, Dr Pablo del Pino, and Dr Oliver Kreft for helpful discussions. This work was supported by the German Research Foundation (DFG, SPP 1313), the European Commission (Nanointeract project), the Comunidad de Madrid S-0505/MAT/0194 and Reference Laboratory SOIMRM, and the Spanish Ministry of Science and Innovation MAT2008-01489 project.

References

1 A. E. T. Merbach, *The Chemistry of Contrast Agents in Medical Magnetic Resonance Imaging*, Wiley, New York, USA, 2001.
2 J. W. M. Bulte and D. L. Kraitchman, *NMR Biomed.*, 2004, **17**, 484.
3 M. G. Harisinghani, K. S. Jhaveri, R. Weissleder, W. Schima, S. Saini, P. F. Hahn and P. R. Mueller, *Clin. Radiol.*, 2001, **56**, 714.
4 Y. M. Huh, Y. W. Jun, H. T. Song, S. Kim, J. S. Choi, J. H. Lee, S. Yoon, K. S. Kim, J. S. Shin, J. S. Suh and J. Cheon, *J. Am. Chem. Soc.*, 2005, **127**, 12387.
5 S. Sun, C. B. Murray, D. Weller, L. Folks and A. Moser, *Science*, 2000, **287**, 1989.
6 M. Corti, A. Lascialfari, E. Micotti, A. Castellano, M. Donativi, A. Quarta, P. D. Cozzoli, L. Manna, T. Pellegrino and C. Sangregorio, *J. Magn. Magn. Mater.*, 2008, **320**, e320.
7 A. Figuerola, A. Fiore, R. Di Corato, A. Falqui, C. Giannini, E. Micotti, A. Lascialfari, M. Corti, R. Cingolani, T. Pellegrino, P. D. Cozzoli and L. Manna, *J. Am. Chem. Soc.*, 2008, **130**, 1477.
8 V. F. Puntes, D. Zanchet, C. Erdonmez and A. P. Alivisatos, *J. Am. Chem. Soc.*, 2002, **124**, 12874–12880.
9 S. Sun, H. Zeng, D. B. Robinson, S. Raoux, P. M. Rice, S. X. Wang and G. Li, *J. Am. Chem. Soc.*, 2004, **126**, 273.
10 S. Sun and H. Zeng, *J. Am. Chem. Soc.*, 2002, **124**, 8204.
11 E. V. Shevchenko, D. V. Talapin, A. L. Rogach, A. Kornowski, M. Haase and H. Weller, *J. Am. Chem. Soc.*, 2002, **124**, 11480.
12 F. Wetz, K. Soulantica, M. Respaud, A. Falqui and B. Chaudret, *Mater. Sci. Eng., C*, 2007, **27**, 1162.
13 A. G. Roca, S. Veintemillas-Verdaguer, M. Port, C. Robic, C. J. Serna and M. P. Morales, *J. Phys. Chem. B*, 2009, **113**, 7033.
14 U. I. Tromsdorf, N. C. Bigall, M. Kaul, O. T. Bruns, M. S. Nikolic, B. Mollwitz, R. A. Sperling, R. Reimer, H. Hohenberg, W. J. Parak, S. Förster, U. Beisiegel, G. Adam and H. Weller, *Nano Lett.*, 2007, **7**, 2422.
15 G. Decher, *Science*, 1997, **277**, 1232.
16 G. Ladam, P. Schaad, J. C. Voegel, P. Schaaf, G. Decher and F. Cuisinier, *Langmuir*, 2000, **16**, 1249.
17 G. B. Sukhorukov, E. Donath, S. Davis, H. Lichtenfeld, F. Caruso, V. I. Popov and H. Möhwald, *Polym. Adv. Technol.*, 1998, **9**, 759.
18 E. Donath, G. B. Sukhorukov, F. Caruso, S. A. Davis and H. Möhwald, *Angew. Chem., Int. Ed.*, 1998, **37**, 2201.
19 B. Radt, T. A. Smith and F. Caruso, *Adv. Mater.*, 2004, **16**, 2184.
20 A. G. Skirtach, A. A. Antipov, D. G. Shchukin and G. B. Sukhorukov, *Langmuir*, 2004, **20**, 6988.
21 M. F. Bédard, D. Braun, G. B. Sukhorukov and A. G. Skirtach, *ACS Nano*, 2008, **2**, 1807.
22 M. F. Bédard, A. Munoz-Javier, R. Mueller, P. del Pino, A. Fery, W. J. Parak, A. G. Skirtach and G. B. Sukhorukov, *Soft Matter*, 2009, **5**, 148.
23 G. B. Sukhorukov, A. L. Rogach, M. Garstka, S. Springer, W. J. Parak, A. Muñoz-Javier, Oliver Kreft, A. G. Skirtach, A. S. Susha, Y. Ramaye, R. Palankar and M. Winterhalter, *Small*, 2007, **3**, 944.
24 P. Rivera Gil, L. L. del Mercato, P. del Pino, A. Munoz Javier and W. J. Parak, *Nano Today*, 2008, **3**, 12.
25 Z. Lu, M. D. Prouty, Z. Guo, V. O. Golub, C. S. Kumar and Y. M. Lvov, *Langmuir*, 2005, **21**, 2042.
26 O. Kreft, A. G. Skirtach, G. B. Sukhorukov and H. Mohwald, *Adv. Mater.*, 2007, **19**, 3142.
27 D. A. Gorin, S. A. Portnov, O. A. Inozemtseva, Z. Luklinska, A. M. Yashchenok, A. M. Pavlov, A. G. Skirtach, H. Mohwald and G. B. Sukhorukov, *Phys. Chem. Chem. Phys.*, 2008, **10**, 6899.

28 S. H. Hu, C. H. Tsai, C. F. Liao, D. M. Liu and S. Y. Chen, *Langmuir*, 2008, **24**, 11811.
29 B. Zebli, A. S. Susha, G. B. Sukhorukov, A. L. Rogach and W. J. Parak, *Langmuir*, 2005, **21**, 4262.
30 C.-A. J. Lin, R. A. Sperling, J. K. Li, T.-Y. Yang, P.-Y. Li, M. Zanella, W. H. Chang and W. J. Parak, *Small*, 2008, **4**, 334.
31 M. T. Fernández-Argüelles, A. Yakovlev, R. A. Sperling, C. Luccardini, S. Gaillard, A. S. Medel, J.-M. Mallet, J.-C. Brochon, A. Feltz, M. Oheim and W. J. Parak, *Nano Lett.*, 2007, **7**, 2613.
32 X. W. Wu, C. Liu, L. Li, P. Jones, R. W. Chantrell and D. Weller, *J. Appl. Phys.*, 2004, **95**, 6810.
33 P. de la Presa, T. Rueda, A. Hernando, J. M. Ramallo-Lopez, L. J. Giovanetti and F. G. Requejo, *J. Appl. Phys.*, 2008, **103**, 103909.
34 M. El-hilo, K. Ogrady and R. W. Chantrell, *J. Magn. Magn. Mater.*, 1992, **109**, L164.
35 J. L. Dormann, L. Bessais and D. Fiorani, *J. Phys. C: Solid State Phys.*, 1988, **21**, 2015.
36 C. Corot, P. Robert, J. M. Idee and M. Port, *Adv. Drug Delivery Rev.*, 2006, **58**, 1471.
37 R. A. Sperling, T. Liedl, S. Duhr, S. Kudera, M. Zanella, C.-A. J. Lin, W. Chang, D. Braun and W. J. Parak, *J. Phys. Chem. C*, 2007, **111**, 11552.

